ELEVENTH EUROPEAN ROTORCRAFT FORUM

Paper No. 30

# A PRESCRIBED WAKE MODEL FOR HELICOPTER ROTOR BEHAVIOUR

H. Azzam and P. Taylor

Department of Aeronautics and Astronautics
University of Southampton
Southampton, U.K.

September 10 - 13, 1985
London, England

THE CITY UNIVERSITY, LONDON, EC1V 0HB, ENGLAND

# A PRESCRIBED WAKE MODEL FOR HELICOPTER ROTOR BEHAVIOUR

H. Azzam, Research Fellow, Southampton University
P. Taylor*, Southampton University, U.K.

## Abstract

The reported prescribed wake models do not describe the rotor behaviour with sufficient accuracy especially at low forward speeds. Meanwhile, the results of the free wake models differ from one to another and yet cannot cover the whole speed range. The objective of this paper is to report the development of an efficient prescribed wake model which describes the rotor behaviour adequately at any flight speed.

The model is validated by comparing results with a set of experimental data collected from different sources. The model is found to predict the flapping angles (including the lateral one), induced power, blade loadings and the instantaneous induced velocities below the rotor adequately.

## Notation

| | | |
|---|---|---|
| $a$ | : | The local lift curve slope. |
| $b$ | : | Number of blades. |
| $c$ | : | Blade chord, metres. |
| $c_T$ | : | Thrust coefficient, $= 2T/(\rho A V_T^2)$ |
| $e$ | : | Flapping hinge offset, nondimensionalized w.r.t. R. |
| $g$ | : | Out of plane mode shape , metres. |
| $h$ | : | Core radius of the tip vortex, metres. |
| $M_a$ | : | Aerodynamic moment about the flapping hinge, Newtons-metre. |
| $m$ | : | Mass per uint length of the blade, kilograms/metre. |
| $n$ | : | Momentum contraction ratio. |
| $n_e$ | : | Effective contraction ratio. |
| $R$ | : | Rotor radius, metres. |
| $T$ | : | Rotor Thrust, Newtons. |
| $V_T$ | : | Rotor Tip speed, metres/second. |
| $V$ | : | Resultant velocity at the rotor disc based on momentum theory, metres/second. |
| $W$ | : | Resultant velocity far downstream based on momentum theory, metres/second. |
| $\beta$ | : | Flapping angle, radians. |
| $\eta$ | : | Time dependent flapwise coordinate, radians. |
| $\theta$ | : | Total pitch angle, radians. |
| $\varepsilon$ | : | Root cut out, nondimensionalized w.r.t. R. |
| $\Gamma$ | : | Strength of the bound circulation, metres$^2$/second. |
| $\gamma$ | : | Strength of a trailing vortex, metres$^2$/second. |
| $\lambda_i$ | : | The momentum induced velocity in forward speed, nondimensionalized w.r.t. $V_T$. |
| $\lambda_{io}$ | : | The momentum induced velocity in hover, nondimensionalized w.r.t. $V_T$. |
| $\lambda_1, \lambda_2$ | : | Tip vortex settling rates, nondimensionalized w.r.t. $V_T$. |
| $\mu$ | : | Local velocity of the air, nondimensionalized w.r.t. $V_T$. |
| $\mu_T$ | : | Tangential component of the local velocity of the air, nondimensionalized w.r.t. $V_T$. |
| $\mu_N$ | : | Normal component of the local velocity of the air, nondimensionalized w.r.t. $V_T$. |
| $\rho$ | : | Air density, kilograms/metre$^3$. |

---

*presently Westland PLC, Yeovil, Somerset

## 1. Introduction

The wake of a helicopter rotor plays an important part in determining the dynamic response of the blades and hence the vibrational forces and moments transmitted to the fuselage. The wake models based on the assumption of an infinite number of blades are computationally efficient. But, they describe an average inflow rather than an instantaneous one. Besides, this inflow is optimistic, and hence the predicted induced power is less than the value expected. On the other hand, the development of the free wake models is restrained by their computational time requirements. The free wake in general is unwittingly prescribed by several parameters which have been introduced to compensate for the discrete representation of the wake and the insensitivity to the dynamics of the rotor. A serious additional problem is the numerical instability of the schemes reported. One reason for this is the lack of representation of cross-flow-vorticity terms. Another is that the relaxation schemes are based on velocity equilibrium only, and not force equilibrium. A third is the absence of an appropriate simulation of the blade vortex interaction and the rolling up process. An adequate free wake model, that is one whose formulation includes the above features, will require large computational times.

The prescribed wake models represent a much faster procedure which is suitable for design purposes and day to day work. The air loads predicted by the undistorted wake models of Miller (1964, ref. 1) and Piziali (1966, ref. 2) were in a good agreement with the experimental data reported by Scheiman (1964, ref. 3). Moreover, Young (1982, ref. 4) demonstrated the capability of the WHL and RAE vortex ring model to predict the rotor loads in forward flight. Nevertheless, the prescribed wake models do not describe the rotor behaviour adequately at low forward speed. Harris (1972, ref. 5) found that the lateral flapping angle predicted by these models differed from the measured values especially at low advance ratios. Later, Johnson (1981, ref. 6) succeeded in predicting the lateral flapping angles accurately by using a free wake model and lifting line theory. He stated that the free wake model is the only way of achieving such an agreement.

The purpose of this paper is to report the development of an efficient prescribed wake model which predicts the flapping response accurately (ref. 7 and 8) and to establish the adequacy of this model in a helicopter rotor performance analysis.

## 2. Description of the Model

Behind a rotating blade, a vortex sheet is generated (the near interactive wake). After leaving the blade, the sheet starts to roll up. Within 30 to 50 degrees azimuth, the roll up process produces a distinguishable tip vortex. No strong physical evidence exists to suggest an inner discrete vortex. Thus, the remaining inboard vorticity is distributed in the inner volume. After a few revolutions, the wake is characterized by instability, turbulent mixing and viscous dissipation.

In order to model the above physical features, the near interactive wake is represented by straight line vortex filaments. The strengths of these filaments are directly related to the local blade loading by using the lifting line theory. The tip vortex co-ordinates are prescribed for any flight regime by using the momentum theory to generalize the experimental results of a rotor in hover. Thus, the contraction and deflection of the wake is introduced. After the point of maximum contraction, the wake is allowed to expand up to one rotor radius. An equivalent core radius of the tip vortex has been defined in order to account for the blade vortex interaction. The relationship defining the equivalent core radius is deduced from a two dimensional vortex-wing interaction model. The strength of the tip vortex has been chosen to be equal to the average of the blade local circulation which is calculated from the dynamic response of the blade. The inboard vorticity is assigned to a single root vortex which emerges from a point behind the rotor centre after the rolling up process is complete. The core of the root vortex is idle (i.e. the induced velocity due to the root vortex inside its core is zero) and its radius is larger than the root cut-out by 0.1 of the rotor radius. The strength of the root vortex is equal and opposite to that of the tip vortex.

## 2.1 The Near Interactive Wake

The near interactive wake is assumed to exist for a number of degrees azimuth corresponding to the time required for the rolling up process to complete. The experimental investigation of a model rotor carried out by Simons et al (1966, ref. 9) shows that the rolling up process is completed in about the time taken to travel a distance equivalent to one rotor radius.

The near interactive wake is represented by straight line vortex filaments positioned midway between the points at which the bound circulations are calculated. The first and last vortex filaments are positioned at the root and the tip of the blade. The strength of each trailed vortex is defined by the difference between the bound circulations at successive radial stations. The lifting line theory is then applied to obtain:

$$\Gamma_i = .5ca_i V_T \left\{ \mu_i \left[ \theta_i + tan^{-1}(\mu_{N1}/\mu_T) \right] - \frac{1}{V_T} \sum_{j=1}^{b(n-1)} \sigma_{ij}\gamma_j \right\} \qquad (1)$$

where:
- "$\Gamma_i$" is the bound circulation at the ith control point,
- "$a_i$" is the local lift curve slope,
- "$\mu_{N1}$" is the normal component of the local velocity of the air which includes the induced velocity due to the tip vortex,
- "$\sigma_{i,j}$" is the influence coefficient of the jth trailing vortex at the ith control point,
- "$\gamma_j$" is the strength of the jth trailing vortex,
- "n" is the number of the control points along the blade,
- "b" is the number of the blades.

The value of the bound circulation at the tip and the root of the blade is zero. Thus, equation 1 represents b(n-2) linear equations which can be solved to obtain the strengths of the bound circulation at each time step. The local lift curve slope is a function of the angle of attack and Mach number which both are dependent on the induced velocity of the near interactive wake. However a first approximation of "a"is estimated by neglecting the effect of the near interactive wake. Then equation 1 is solved to determine the bound circulations and hence, the induced velocities due to the near wake. These induced velocities are used to recalculate better values of "$a_i$". The procedure is then repeated to converge "$a_i$" and "$\Gamma_i$" together.

## 2.2 The Strength of the Tip Vortex

The strength of the tip vortex used in most of the wake models is chosen to be equal to the maximum value of the blade bound circulation. The basic disadvantages of this are the sensitivity to the location of the control points, the wake geometry and the core radius of the tip vortex. Thus, additional computational time is required to match the tip vortex strength with the maximum bound circulation of the blade. Moreover, the experimental investigation of Cook (1972, ref. 10) showed that the circulation contained in the tip vortex is less than the peak circulation near the blade tip.

Instead, the strength of the tip vortex is chosen to be equal to the following average of the bound circulations of the blade:

$$\Gamma_a(\psi) = \int_\varepsilon^1 (x-e)\mu_T \Gamma(r,\psi)dx \Big/ \int_\varepsilon^1 (x-e)\mu_T dx \qquad (2)$$

where:
- "$\varepsilon$" is root cut out,
- "e" is the flapping hinge offset,
- "$\mu_T$" is the tangential component of the local velocity of the air,
- "x" is the non-dimensionalized radial coordinate,
- "$\psi$" is the azimuth coordinate.

Thus, more weight has been given to the bound circulations in the blade tip region in which the bound circulations reach a maximum value. Now, the aerodynamic moment about the flapping hinge; "$M_a$" can be related to the tip vortex strength as follows:

$$M_a = \rho R^2 V_T \Gamma_a(\psi) \int_\varepsilon^1 (x-e)\mu_T dx \tag{3}$$

On the other hand, the aerodynamic moment is a direct function of the dynamic response of the blade. For example, assuming uncoupled out of plane motion gives:

$$M_a = \sum_k (\eta_k'' + \nu_k^2 \eta_k)\Omega^2 \int_o^{R-eR} m g_k(r) r dr \tag{4}$$

where: "$g_k$" is the kth flapwise mode shape,
"$\eta_k$" is the kth time dependent co-ordiate (the flapping angle for the first mode)
"$\nu_k$" is the associated natural frequency,
"r" is a radial co-ordinate; = 0 at the flapping hinge,
"m" is the mass per unit length of the blade
"$\Omega$" is the angular velocity of the rotor

Thus, the harmonics of the dynamic response are transmitted to the tip vortex through the weighting function of equation 2. Equation 4 is also valid for a hingeless blade (e = 0). Considering the first mode shape to be a straight line, the integral in equation 4 reduces to the second moment of mass of the blade.

2.3 The Tip Vortex Co-ordinates

The tip vortex co-ordinates are generated by integrating the formulae for the local velocities of the air at the blade tip after having replaced the instantaneous induced velocities by arbitrary vertical settling rates. The constant radius of the wake is then replaced by an instantaneous contracting radius. The next step is to choose the appropriate values of the settling rates and the instantaneous radius at the required flight regime.

The experimental investigation of a hovering rotor (ref. 11 and 12) suggests the following empirical formula for the instantaneous radius; "$r_i$" of the tip vortex;

$$r_i/R = \sqrt{n_e} + (1 - \sqrt{n_e})\, e^{-\lambda \Psi_w} \tag{5}$$

where: "$\psi_w$" is the wake azimuth angle relative to the blade,
"$\lambda$" is constant depending on the rotor parameters.

"$n_e$" may be considered as an effective contraction ratio. Meanwhile, the momentum theory can be used to define the contraction ratio "n" at any forward speed as follows:

$$n = V/W \tag{6}$$

where: "V" is the resultant velocity at the rotor disc,
"W" is the resultant velocity far downstream.

Now the effective contraction ratio at any forward speed is assumed to be a linear function of the momentum contraction ratio:

$$n_e = .7832n + .2168 \tag{7}$$

Furthermore, the experimental investigations of a hovering rotor indicate the existence of three settling rates:

- the tip vortex axial settling rate over the interval from the vortex formation to the following blade passage "$\lambda_1$".
- the tip vortex axial settling rate over the interval from the following blade passage to the point of maximum wake contraction "$\lambda_2$".
- the unstable axial settling rate after the point of maximum wake contraction.

In order to extend the experimental results of a rotor in hover to cover the forward speed range, the settling rates are related to the contraction ratios through the following relations:

$$\lambda_1 = \lambda_i \left[ 1 - K_1 (\frac{n_e}{n} - 1) \right] \tag{8}$$

$$\lambda_2 = \lambda_i \left[ 1 - K_2 (\frac{n_e}{n} - 1) \right] \tag{9}$$

where: "$\lambda_i$" is the momentum induced velocity.

The constants "$K_1$" and "$K_2$" are selected such that the settling rates correspond to the experimental values in hover.

Equations 7, 8 and 9 are justified because of the following:

1. At hover ($n = .5$ and $n_e = .6084$) the instantaneous radius of the wake and its settling rates correspond to the experimental values.
2. As the forward speed increases, the momentum contraction ratio approaches unity and consequently the effective contraction ratio approaches unity. Also the values of the settling rates approach the value of the momentum induced velocity. Thus, the tip vortex co-ordinates approach those of the above reported prescribed wake models (references 1, 2 and 4) which were found to represent the rotor behaviour at forward speed adequately.

The values of "$\lambda$", "$\lambda_1$" and "$\lambda_2$" at hover used in the wake model are those proposed by Kocurek and Tangler (1977, ref. 12). The wake below the point of maximum contraction is assumed to be stable and is allowed to expand up to one rotor radius by the same contraction rate "$\lambda$". The tip vortex trajectory is dependent on the flapping response not only because of the effect of the flapping on the instantaneous local velocity of the air at the blade tip, but also because of the instantaneous position of the blade tip relative to the hub plane. Meanwhile, the settling rate "$\lambda_1$" is less than the momentum induced velocity. Thus, the tip vortex may pass over or encounter the following blade.

## 2.4 The Blade Vortex Interaction

A typical experimental value of the tip vortex core radius is 10% of the blade chord. Nevertheless, if this value is used, large induced lift coefficients may result. Meanwhile, the experimental investigation of Ham (1975, ref. 13) indicated that the maximum vortex induced lift coefficient is limited to a value of the order of .2 to .3. Ham also found that the measured induced load on the blade differed greatly from that predicted by the lifting surface theory (1974, ref. 14). Egolf and Landgrebe (1983, ref. 15) found that the current lifting surface models are not sufficient for close blade-vortex interaction modelling because non-linear viscous phenomena, such as vortex induced separation, are neglected. They also found that the most successful representation of the blade-vortex interaction in the wake models is the hypothetical large core representation of the tip vortex suggested by Scully (1975, ref. 16). In several wake models, the equivalent core radius is chosen to be a unique value for the speed range. Nevertheless, if this approach is interpreted as an economic tool to control the maximum induced lift, then the value of the core radius is expected to change with the rotor parameters and flight speeds. The purpose of this section is to develop a parametric relationship for the equivalent core radius of the tip vortex.

Gangwani (1983, ref. 17) stated that the close interaction of a concentrated free vortex with a lifting surface can be separated into two mechanisms; the first is the influence of the vortex induced velocity field, and second is the suction effect which results from the low pressure region within the vortex. By considering a two dimensional vortex passing below a wing whose span is perpendicular to the centre line of the vortex and using the method of images, the suction load "$\Delta T_s$" on the wing becomes:

$$\Delta T_s \alpha \rho \Gamma^2 \frac{c}{Z} \tag{10}$$

where "$\Gamma$" is the strength of the vortex
"c" is the wing chord
"Z" is the distance of the vortex below the wing.

Since only a parametric equation is required, then it can be assumed that the induced load "$\Delta T_i$" is proportional to "$\Gamma$":

$$\Delta T_i \alpha \Gamma \rho V_T c \tag{11}$$

Now by choosing the equivalent core such that the local maximum induced velocity, and hence the induced load do not exceed a reference velocity (the reference velocity is chosen to be proportional to the momentum induced velocity at hover "$\lambda_{io}$")

$$h \alpha \frac{\Gamma}{\lambda_{io} V_T} \tag{12}$$

where "h" is the equivalent core radius.
The induced load is related to "h" by:

$$\Delta T_i \alpha \lambda_{io} V_T^2 h \rho c \tag{13}$$

The steady part of the tip vortex strength of a rotor given by reference 4 is:

$$\Gamma \simeq \frac{2T}{\rho b V_T R} \tag{14}$$

where: "T" is the rotor thrust.

It is assumed that the relationships 10 and 13 are valid for a helicopter rotor and, furthermore that the induced load calculated by the Biot Savart law for a given wake follows the form of relationship 13. It is required now to bring the calculated induced load as close as possible to the values of the actual suction and induced loads. Hence, the relatioships 10, 13 and 14 give:

$$h \alpha \frac{R^2 C_T^{1.5}}{b^2 Z} \tag{15}$$

The remaining task is to estimate a value for the vertical distance "Z" of the tip vortex below the preceding blade. Fortunately, this distance is proportional to the momentum induced velocity in the above wake representation. Thus:

$$h \alpha \frac{C_T^{1.5}}{b\lambda_i} \tag{16}$$

The constant of proportionality is chosen to be "1.85" which has been found to give a smooth variation of the induced power factor with the thrust coefficient at hover. Some values of this constant resulted in values of the induced power factor which were less than unity at low thrust coefficiencts.

## 3. The Computer Program Description

The above equations have been implemented in a computer program called RWAKE. At this stage, the first flapwise mode shape is approximated to a straight line and the flapping motion only is considered. For a given rotor behaviour calculation the input of the program is the required thrust, cyclic control angles and velocity state. The thrust coefficient and the number of the blades are used to calculate the tip loss factor. The control points are distributed along the blade, being concentrated towards the tip. The control point No. n-1 is positioned at a distance equal to the square of the tip loss fctor. This choice is a simple way of accounting for the three dimensional effects as described in ref. 7. At the control points No. 1 and n, zero values are assigned to the aerodynamic forces.

The thrust coefficient and the cyclic control angles are used to calculate the momentum induced velocity and initial values for the collective and flapping angles. This information is used to establish the initial wake geometry and the strength of the tip vortex. Thus, the contribution of the tip vortex to the induced velocity is determined. Equation 1 is used to calculate the bound circulation of the blade for the initial value of the collective pitch angle as described above. The instantaneous induced velocity profile is then obtained.

The value of the thrust is checked and the collective pitch angle is adjusted to obtain the required thrust without changing the induced velocity profile.

New estimates of the local flapping angles, which is consistent with the current induced velocity profile and control angles are obtained by using a rapidly convergent technique based on curve fitting. The aerodynamic moment about the flapping hinge is calculated at different azimuth positions by using the old estimates of the flapping angles. The parts of the aerodynamic moment which are dependent on the flapping angle and its derivative are divided by the old estimates of the local flapping angle and its derivative respectively to define two sets of local coefficients. The flapping equation is rewritten such that these coefficients multiplied by the required flapping angle and its derivative appear at the left hand side of the equation. The No. of the coefficients of the Fourier expansion of the flapping angle is chosen to be equal to the number of the azimuth positions around the rotor disc. The flapping equilibrium equation is then satisfied at each azimuth station. Thus, a system of linear equations are obtained and solved to evaluate new estimates of the flapping coefficients. The new values of the flapping angles are used to recalculate the aerodynamic moments and the local coefficients. This procedure is repeated until the required precision is obtained.

The value of the thrust for the new flapping angles is checked, and the collective pitch angle is adjusted to obtain the required thrust. The flapping calculation is then repeated. The above iterations result in consistent values of collective pitch and flapping angles for the initial induced velocity profile.

The new estimate of the flapping response are used to establish the wake geometry and the strength of the tip vortex. The bound circulations are then recalculated and a new velocity profile is obtained.

The above procedure is repeated until the collective pitch angle, the flapping response, and the induced velocity profile have all converged.

4. Comparison With Experimental Data

The purpose of this section is to validate the above model by comparing its results to a set of experimental data collected from different sources.

Figure 1 shows typical performance results of a model rotor in hover. The agreement between the theory and the test of reference 12 is satisfactory. However, a difficult task was the choice of the proper two dimensional aerofoil data. Such data is a function of Reynolds number, Mach number, surface roughness, and the particular shape of the leading and trailing edges. The two dimensional data from reference 18 (Gregory and Wilby, 1973) was used. Nevertheless, one or two experimental data points have been used to scale this data. It was found that scaling of the lift independent drag coefficient was necessary to obtain a reasonable profile power. At this point, it may be argued that this scaling is equivalent to synthesizing the aerodynamic coefficients for a given induced velocity profile. Therefore, the next step is to examine the values of the induced power factor which are an integral measure of both the induced velocity profile and the lift distribution. Figure 2 shows that the calculated induced power factor is greater than unity. As expected, an increase in the thrust coefficient causes a rise in the induced power factor. Also, the induced power factor reduces with an increase in the number of blades for the same thrust coefficient. Now, to increase the degree of confidence in the model, the induced velocities below a rotor in hover have been predicted; figure 3. The results of prescribed wake model displaying a closer agreement with the measured induced velocities of reference 19, compared to the free wake method presented in the same reference. The difference in the upwash induced velocities should be expected since the experimental wake contraction was not symmetrical because of the wind tunnel wall interference effects.

The next step is to examine the validity of the model in forward speed. Figures 4 to 6 show comparison between the calculated flapping angles and those measured by Harris (reference 5). The accuracy of the measurements was 0.25 degrees. The experimental value of the power in hover is used to scale the lift independent drag coefficient. It is clear that the prescribed wake model is capable of predicting the value of the lateral flapping angle at low forward speed. The only reported wake model having the same capability is the free wake model of Johnson (ref. 6) which does not converge below .04 advance ratio. The lateral flapping angle is sensitive to the induced velocity profile. Therefore the agreement with the experimental data suggests that the induced velocity profile of the prescribed wake model is reasonable. The measured and calculated power and H-force for the same model rotor are presented in figures 7 and 8. The agreement between the theory and the test may be regarded as and indication of a reasonable induced velocity and lift distributions. Furthermore, the induced power factors are always greater than unity. The calculated values of the collective pitch angles are found to have exactly the same trend, but lower than the measured values. Johnson also found that the calculated collective pitch angles are less than the measured values. He attributed that to the elastic pitch deflection of the blade. Meanwhile, figure 9 shows that the prescribed wake model succeeded to predict accurately the collective pitch angle for a typical two bladed tail rotor at hover (ref. 7). Nevertheless, the control system and the blade were exceptionally stiff.

The next step is to examine the local effects of the wake model at forward speed. Therefore, the blade loading is evaluated and compared to the flight test data of Scheiman and Ludi (1963, ref. 20), figure 10. The overall agreement with the flight test data is satisfactory. The model does not allow for the interference effects of the tail-rotor or the fuselage. Thus, a difference between the test and the theory is expected at the inboard portion of the blade when the blade passes over the fuselage. A difference is also expected when the blade tip moves in the vicinity of the tail rotor. It is worth mentioning that the unsteady effects are not included in the model at this stage.

Nevertheless, the model predicts the airloading with at least the same accuracy of the prescribed wake models of Miller and Piziali (ref. 1 and 2) which allowed for the unsteady effects.

The induced velocities below a four bladed model rotor at 0.1 advance ratio is calculated and compared to the experimental data of reference 21. The overall agreeement with the test is reasonable; figure 11. Meanwhile, the difference in the harmonic contents of the induced velocity profile when the hot wire probe was behind the hub may be attributed to the hub wake as well as to the simple representation of the inboard vortex sheet. The traces of the induced velocity when the hot wire probe was at 270 degrees azimuth are shown in figure 12 for different radial positions. These traces indicate that the theoretical tip vortex trajectory is slightly different from the experimental one. A good agreement between the theory and the test is found for the probe positions which are just outside the wake (e.g. at r/R = 1.1, figure 12). This is an indication that the strength of the tip vortex is appropriately estimated.

## 5. Concluding Remarks

The development of an efficient prescribed wake model has been reported. The wake is allowed to contract and deflect. The strength of the tip vortex is related to the dynamic response of the blade. The three dimensional effects and blade-vortex interaction have been accounted for simply. The capability of this model to describe the rotor behaviour adequately at any flight regime has been demonstrated. The correlation of the computed and measured results is reasonable. The model is found to predict the flapping angles (including the lateral one), induced power, blade loadings and the induced velocities below the rotor adequately.

## REFERENCES


1. R.H. Miller, Unsteady Air Loads on Helicopter Rotor Blades, Journal of the Royal Aeronautical Society, April 1964.
2. R.A. Piziali, Method for the Solution of the Aeroelastic Response for Rotating Wings, Journal of Sound and Vibration, Vol. 4 No. 3, 1966.
3. J. Scheiman, A Tabulation of Helicopter Rotor-Blade Differential Pressures, Stresses and Motions as Measured in Flight, NASA TMX-952, 1964.
4. C. Young, Development of the Vortex Ring Wake Model and its Influence on the Prediction of Rotor Loads, AGARD-PP-334, 1982.
5. F.D. Harris, Articulated Rotor Blade Flapping Motion at Low Advance Ratio, Journal of the A.H.S. January 1972.
6. W. Johnson, Comparison of Calculated and Measured Helicopoter Lateral Flapping Angles, Journal of the A.H.S. April 1981.
7. H. Azzam and P. Taylor Investigation of Helicopter Twin-Tail Rotor Characteristics, Southampton University, AASU Memo 83/6, 1983.
8. H. Azzam and P. Taylor Investigation of Helicopter Twin-Tail Rotor Characteristics, Southampton University, AASU Memo 84/19, 1984.
9. I.A. Simons., R. Pacifico, and J.P. Jones The Movement, Structure and Breakdown of Trailing Vortices from a Rotor Blade, CAL/USAAVLABS Symposium Proceeding, Vol. 1, 1966.
10. C.V. Cook, The Structure of the Blade TipVortex, AGARD-CP-111, 1972.
11. A.J. Landgrebe, The Wake Geometry of a Hovering Helicopter Rotor and Its Influence on Rotor Performance, Journal of the A.H.S., October 1972.
12. J.D. Kocurek and J.L. Tangler A Prescribed Wake Lifting Surface Hover Performance Analysis, Journal of the A.H.S., January 1977.
13. D. Ham, Some Conclusions from an Investigation of Blade-Vortex Interaction, Journal of the A.H.S., October 1975.
14. D. Ham, Some Preliminary Results from an Investigation of Blade-Vortex Interaction, Journal of the A.H.S., April 1974.
15. T.A. Egolf, and A.J. Landgrebe Helicopter Rotor Wake Geometry and Its Influence, Vol. 1, NASA CR 3726, 1983.

16. M.P. Scully, Computation of Helicopter Rotor Wake Geometry and its Influence on Rotor Harmonic Airloads, M.I.T., ASRL-TR-178-1, March 1975.
17. S.T. Gangwani, Calculation of Rotor Wake Induced Empennage Airloads, Journal of the A.H.S., April 1984.
18. N. Gregory and P.G. Wilby NPL 9615 and NACA 0012 A Comparison of Aerodynamic Data, ARC, CP No. 1261, 1973.
19. J.M. Pouradier and E. Harowitz Aerodynamic Study of Hovering Rotor, Vertica, Vol. 5, 1981.
20. J. Scheiman, and L.H. Ludi Qualitative Evaluation of Effect of Helicopter Rotor-Blade Tip Vortex on Blade Airloads, NASA TND-1637, 1963.
21. V.G. Sekaran and C. Haddow Result of Instantaneous Induced Velocity Measurements from a Helicopter Rotor Model, Southampton University, AASU Memo 84/6, 1984.

Acknowledgement

The support of Procurement Executive, Ministry of Defence is gratefully acknowledged.

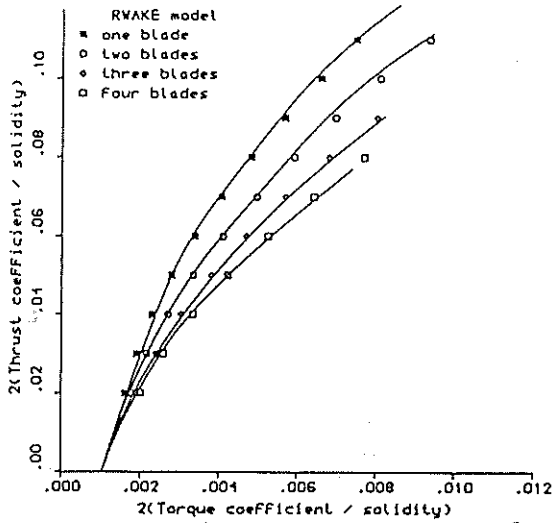


FIG.1 THE CURVES OF A ROTOR PERFORMANCE IN HOVER

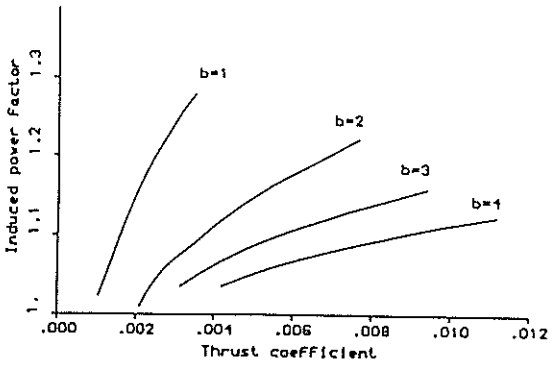


FIG.2 THE CURVES OF THE INDUCED POWER FACTOR

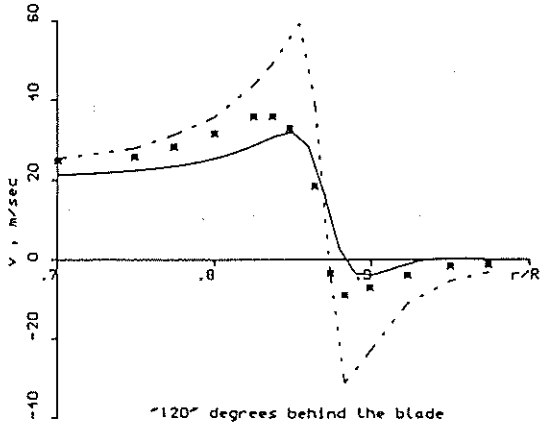


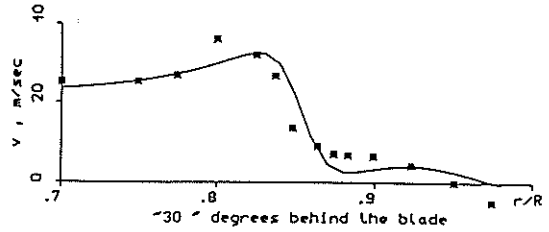


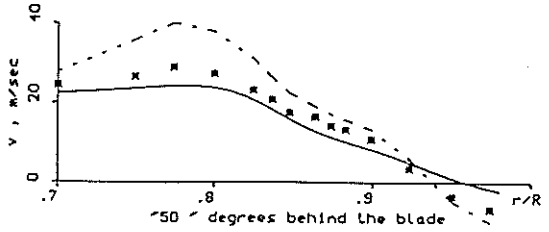


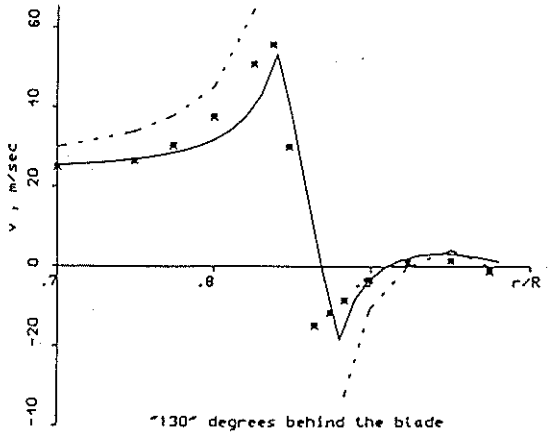


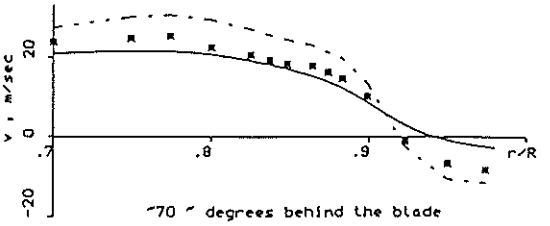


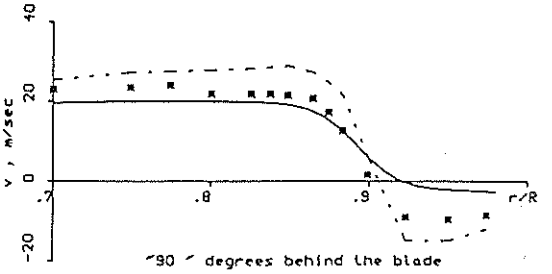


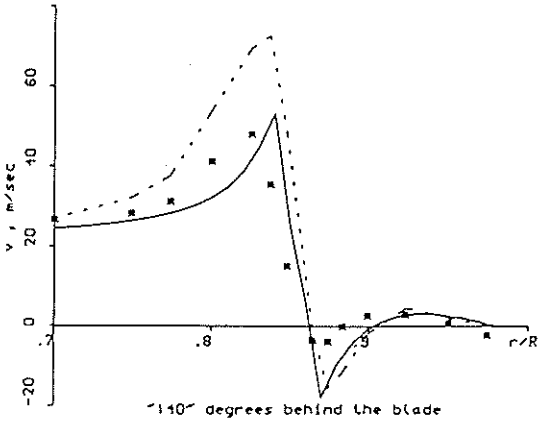


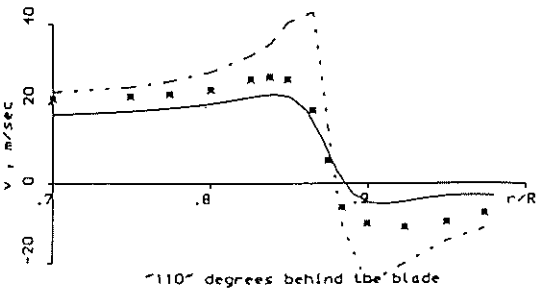


FIG.3 INSTANTANEOUS INDUCED VELOCITY IN HOVER
b=3 C =0.0206 Z/R=0.0677
* Experimental data - RWAKE model .. Ref.19 free wake

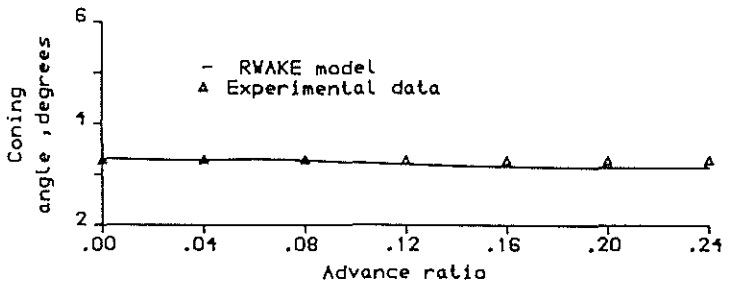


FIG.4 CONING ANGLE IN FORWARD SPEED

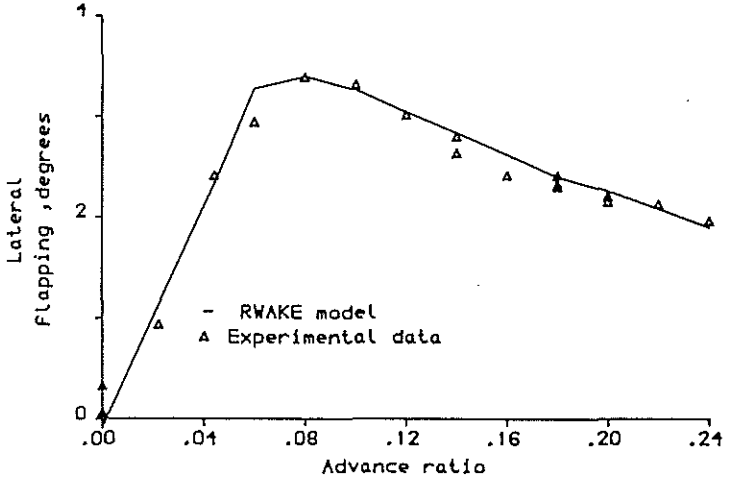


FIG.5 LATERAL FLAPPING IN FORWARD SPEED

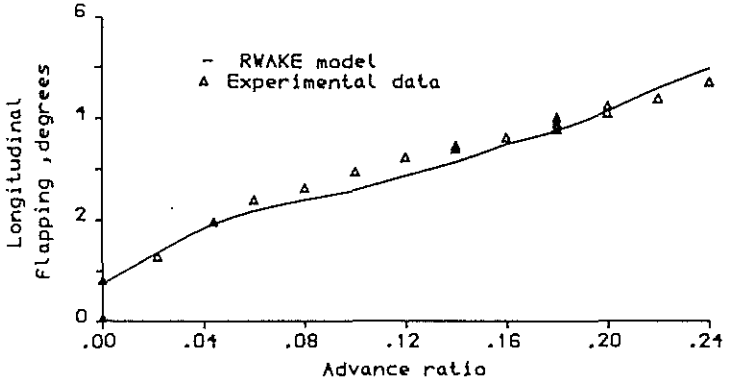


FIG.6 LONGITUDINAL FLAPPING IN FORWARD SPEED

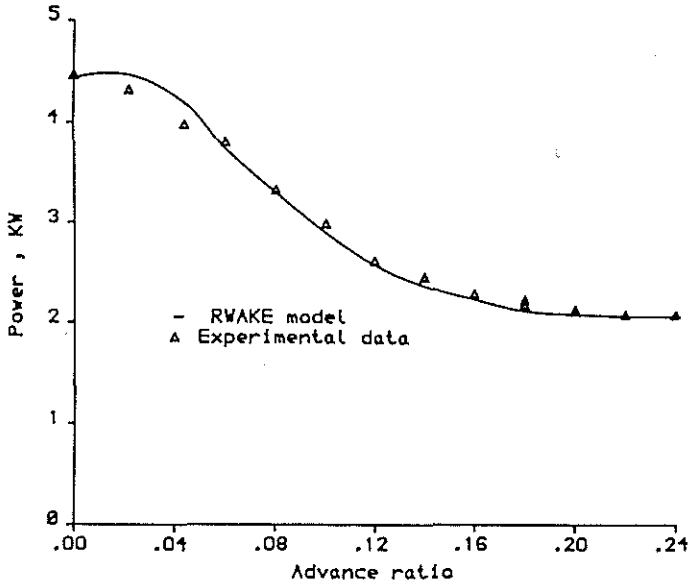


FIG.7 ROTOR POWER IN FORWARD SPEED

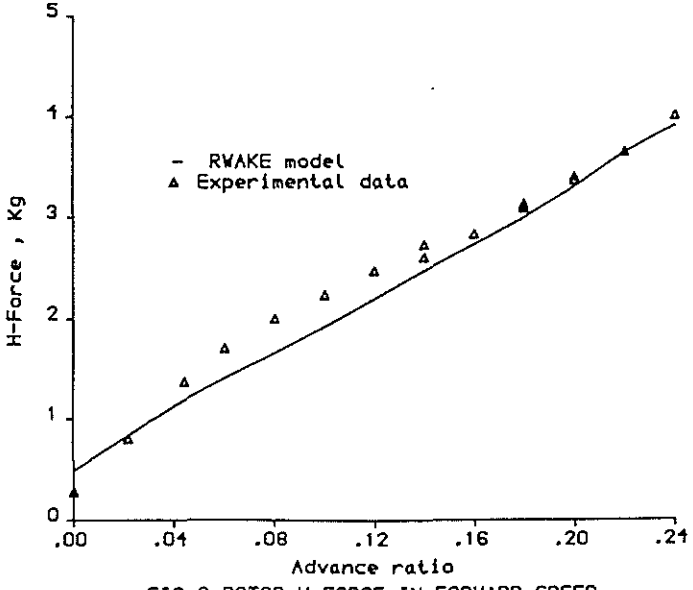


FIG.8 ROTOR H-FORCE IN FORWARD SPEED

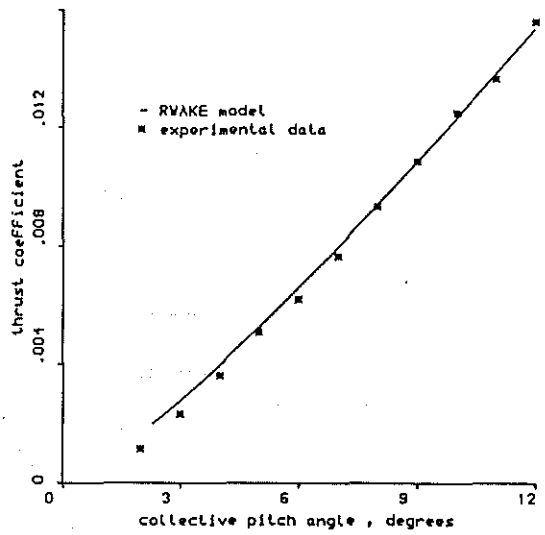


FIG.9 THRUST COEFFICIENT OF TAIL ROTOR IN HOVER

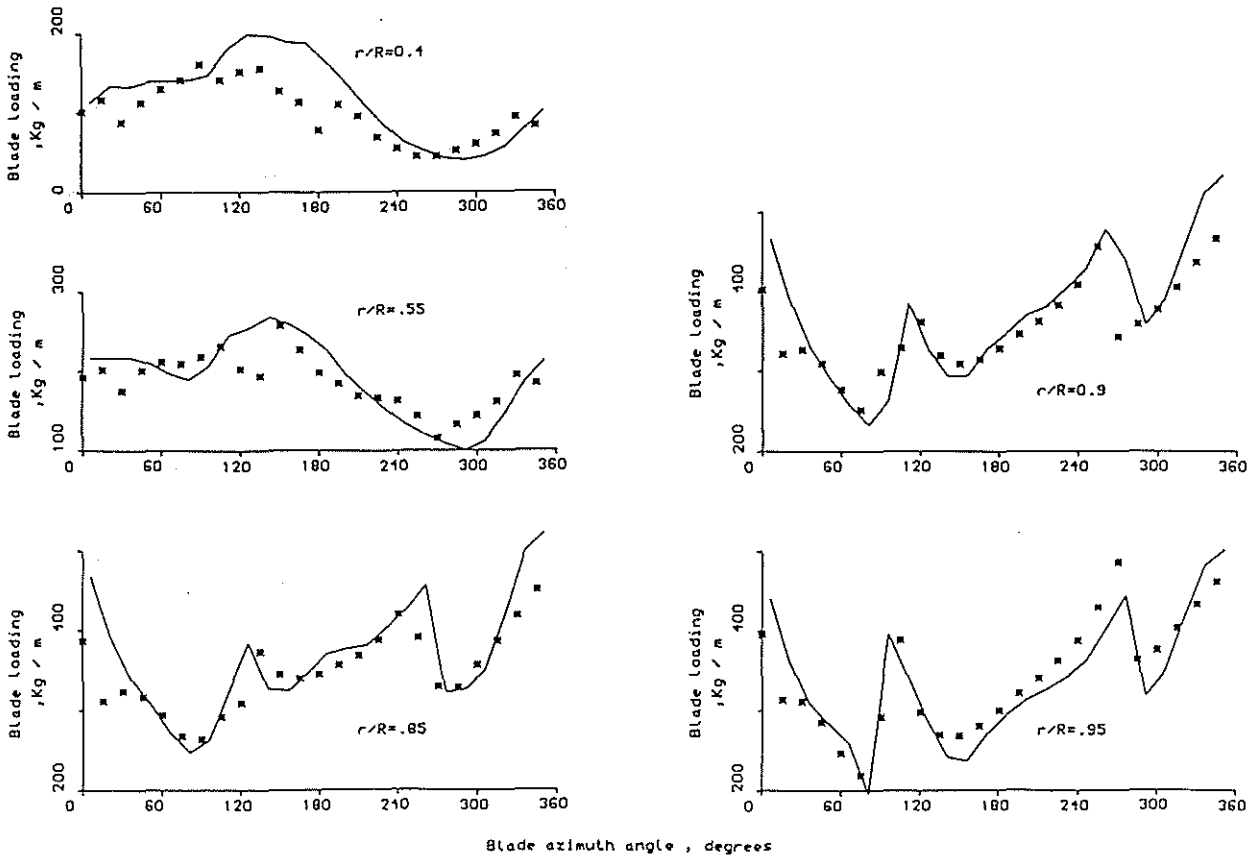


FIG.10 BLADE-SECTION LOADING AT ADVANCE RATIO OF 0.18
* RWAKE model - FLIGHT TEST

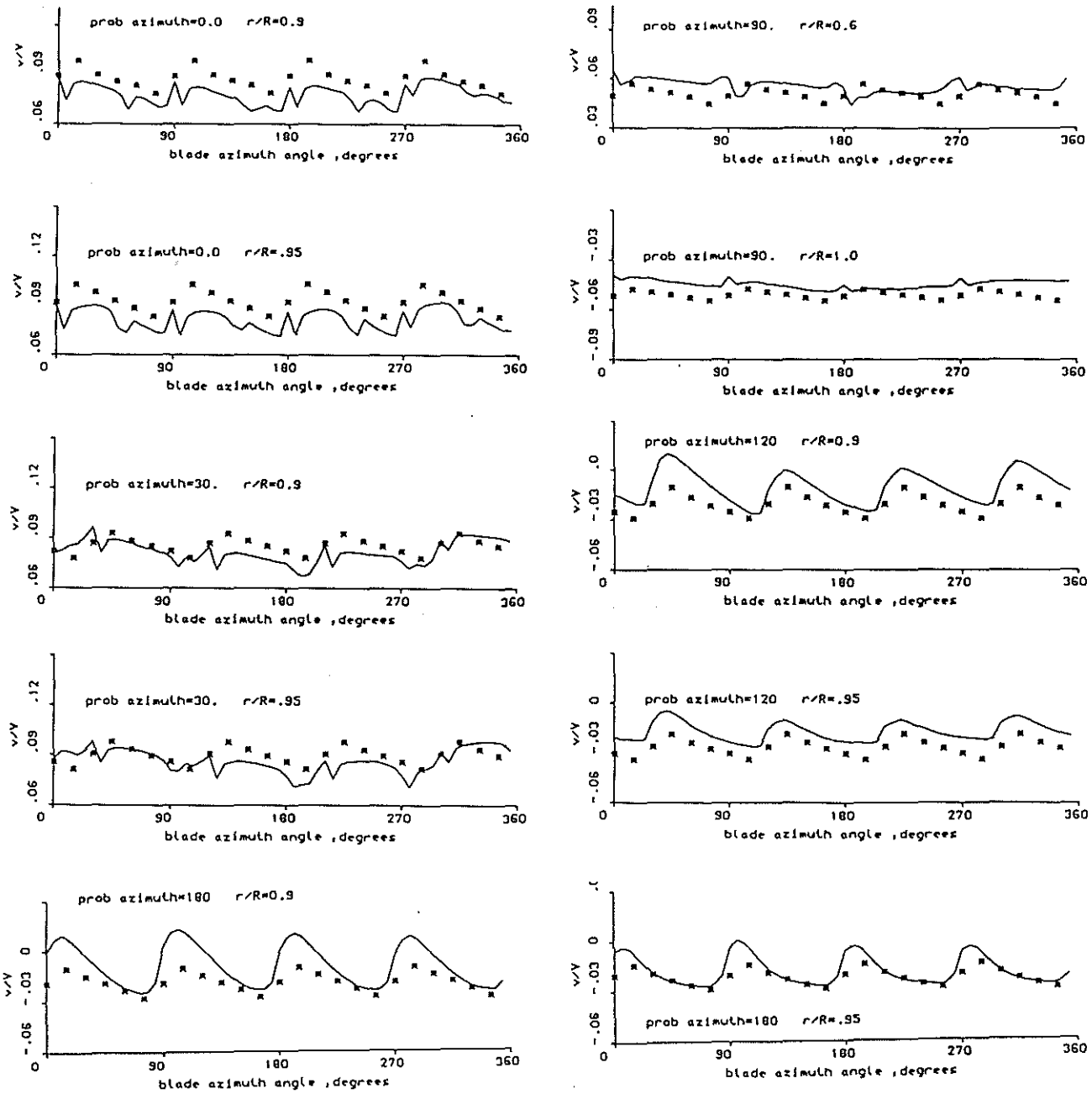


FIG.11 INSTANTANEOUS INDUCED VELOCITY AT ADVANCE RATIO OF 0.1
b=4 C =0.0146 z/R=0.075
* RWAKE model - Experimental data

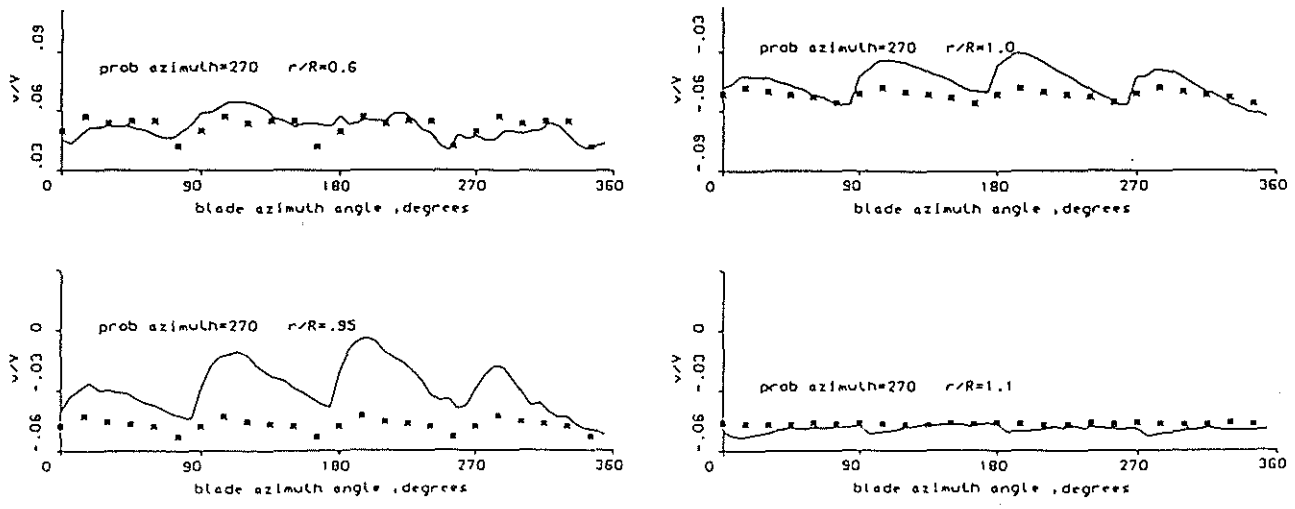


FIG.12 INSTANTANEOUS INDUCED VELOCITY AT ADVANCE RATIO OF 0.1
b=4 C =0.0146 z/R=0.075
* RWAKE model - Experimental data